HiCIRF: A high-fidelity HF channel simulation

L. J. Nickisch,[1] Gavin St. John,[1] Sergey V. Fridman,[1] Mark A. Hausman,[1] and C. J. Coleman[2]

Received 22 November 2011; revised 9 March 2012; accepted 13 March 2012; published 26 April 2012.

[1] A high-fidelity HF channel simulation has been developed that is suitable for Over-the-Horizon Radar (OTHR) and HF communication system design studies and test planning. The simulation capability is called HiCIRF, for High-frequency Channel Impulse Response Function. HiCIRF provides simulated HF signals corresponding to transmissions from individual transmitter array elements to individual receiver array elements for propagation through the naturally disturbed or undisturbed ionospheric channel. Both one-way link geometries and two-way radar geometries can be simulated. HiCIRF incorporates numerical ray tracing and stochastic signal structure computations to realistically simulate signal scatter by small-scale ionization structure. Stochastic signal generation is employed to generate signal realizations that can be used for OTHR array design and advanced signal processing studies.

Citation: Nickisch, L. J., G. St. John, S. V. Fridman, M. A. Hausman, and C. J. Coleman (2012), HiCIRF: A high-fidelity HF channel simulation, *Radio Sci.*, *47*, RS0L11, doi:10.1029/2011RS004928.

1. Introduction

[2] A new simulation capability called HiCIRF, for High-frequency Channel Impulse Response Function, has been developed that is suitable for Over-the-Horizon Radar (OTHR) and HF communication system design studies and test planning. HiCIRF provides simulated HF signals corresponding to transmissions from individual transmitter array elements to individual receiver array elements for propagation through the naturally disturbed or undisturbed ionospheric channel. Both one-way link geometries and two-way radar geometries can be simulated. HiCIRF incorporates numerical ray tracing and stochastic signal structure computations to realistically simulate signal scatter by small-scale ionization structure. Stochastic signal generation is employed to generate signal realizations that can be used for OTHR array design and advanced signal processing studies.

[3] High-fidelity HF channel simulation is important because it allows HF system design studies to be performed inexpensively without having to field prototype systems for testing. For example, imagine the cost of field testing multiple two-dimensional OTHR antenna array configurations involving hundreds of antenna elements under a variety of ionospheric conditions, including conditions with small-scale ionization disturbances that cause angular signal spreading and signal coherence losses that may affect advanced signal processing methods. HiCIRF provides a signal generation capability at the individual antenna element level that can be applied on a pulse-by-pulse or sample-by-sample basis, yet retains the interelement phase characteristics to allow antenna array analyses to be performed.

[4] HiCIRF is a MATLAB-based tool incorporating a number of state-of-the-art propagation algorithms. Basic propagation mode structure is computed using fast two-dimensional numerical ray tracing in a climatological ionosphere model [*Coleman*, 1997, 1998]. Signal strength computations include D region absorption, focusing, ground bounce, and backscatter losses. A land/sea map distinguishes ground backscatter from returned ocean Bragg spectra. Scattering effects (scintillation) are computed using the Phase screen/Diffraction Method [*Nickisch*, 1992] with small-scale ionization structure supplied by WBMOD [*Secan*, 2004].

[5] This article will be limited to an overview of HiCIRF's ingredients and capabilities. Details of the models included in HiCIRF as well as results of validation testing can be found in our interim technical reports on HiCIRF [*Knepp et al.*, 2010, 2011, 2012]. (Extensive validation testing of HiCIRF will be performed in the next year. A final technical report covering HiCIRF development and testing will be available in early 2013, which will be published by our sponsor.)

[6] The paper is organized as follows. In section 2 we discuss the components that make up HiCIRF. Section 3 covers theoretical aspects of simulating HF propagation. Section 4 provides examples of HiCIRF one-way link propagation, and section 5 provides an example of HiCIRF two-way (OTH radar) propagation. Concluding remarks are made in section 6.

2. HiCIRF Components

[7] Realistically simulating HF sky wave propagation in HiCIRF requires the integration of several state-of-the-art

[1]NorthWest Research Associates, Monterey, California, USA.
[2]Electrical and Electronic Engineering Department, University of Adelaide, Adelaide, South Australia, Australia.

0048-6604/12/2011RS004928

propagation and modeling modules. Basic HF propagation mode structure is obtained by numerical ray tracing in a climatological ionosphere model. Ionospherically induced Doppler shifts are incorporated by evaluating temporal ray mode dependence in the evolving background ionosphere model. Signal scatter effects are computed using the theory of stochastic wave propagation in the environment predicted by WBMOD, a climatological model for naturally occurring small-scale ionization structure [*Secan*, 2004]. Doppler spreading of scattered fields is incorporated through the use of plasma drift models. These important HiCIRF elements are discussed in this section.

2.1. Numerical Ray Tracing

[8] We employ the Haselgrove ray tracing codes developed by *Coleman* [1993, 1997, 1998] in both two-dimensional (range and height) and three-dimensional magnetoionic versions. These codes are probably the fastest numerical Hamiltonian-based ionospheric ray tracing codes in the world, which makes them particularly desirable for the computationally intensive simulation application. The extremely fast 2D code is used for components in HiCIRF that require less fidelity (clutter and noise calculations) and the 3D code is used for target signal injection. For one-way link geometries, we have developed a ray homing technique that finds all propagation modes connecting a given transmitter and receiver. For the two-way (radar) geometry, we have developed algorithms for finding all connecting return paths from each outbound hop for separated transmitter and receiver locations.

2.2. Small-Scale Ionization Structure

[9] The goal of HiCIRF is to provide a simulation of the HF channel that can be used to generate HF signal realizations. An important aspect of the HF channel is the effect of small-scale ionization structure that causes signal decorrelation in space, frequency, and time. We have developed modules for these stochastic random media propagation calculations. These modules are based on FORTRAN code that is callable by MATLAB using the MATLAB MEX utilities. The use of compiled FORTRAN MEX modules allows these numerically intensive calculations to be performed with computational speed that could not be attained in a normal MATLAB script.

[10] The climatology of naturally occurring small-scale ionization structure is available in the software package WBMOD [*Secan*, 2004]. We have extracted from WBMOD the subset of subroutines that are required for HiCIRF and made a MATLAB MEX module of them. We have constructed a module that samples the WBMOD-predicted structure along rays for passage to our channel realization module (discussed below).

2.3. Plasma Drift Model

[11] We have incorporated the ionospheric plasma drift velocity model from WBMOD, which combines the Richmond-NCAR (mid-low latitude) and Heelis-UTD (high latitude) plasma convection models [*Richmond et al.*, 1980; *Hairston and Heelis*, 1990]. These models capture the nighttime equatorial eastward drift of 100–150 m/s and the km/s-scale plasma drifts in the polar region. The equatorial drift combined with the strong nighttime equatorial small-scale ionization structure is responsible for the bulk of Spread Doppler Clutter (SDC) observed by OTHRs looking toward the equator.

3. Theoretical Considerations

[12] The output of HiCIRF is the Channel Impulse Response Function that applies the effect of the ionospheric channel on propagating waveforms through convolution. Realizations of the impulse response function can be generated using the Generalized Power Spectral Density (GPSD) function of the propagation channel, and in this section we describe this relationship.

[13] There is a specialized, but rich literature on the development of radiowave scattering theory in structured ionization. References to this literature can be found in the works by *Nickisch* [1992], *Dana and Wittwer* [1991], and *Gherm et al.* [2005]. The work of *Gherm et al.* [2005] is specifically directed toward the HF applications targeted here, but is restricted to the weak-scatter regime for the scattering effects of small-scale ionization structure through their application of an extended Rytov approximation [*Rytov et al.*, 1978]. The theory we apply in HiCIRF, that of *Nickisch* [1992], invokes certain strong-scattering assumptions which are valid for the description of the equatorial and polar/auroral Spread Doppler Clutter (SDC) that affects HF OTH radar. In order to blend this strong-scattering theory with the weak-scatter regime appropriate, for example, to OTH radar path segments in midlatitudes, we take a Rician approach that we will also describe below. Also, as discussed by *Nickisch* [1992], applying phase screen/diffraction method (PDM) as we do in HiCIRF, using the spherical wave version of the parabolic wave equation, neglects certain effects associated with the refraction in the background ionosphere model. We account for variation along the propagation path of important factors that have to do with the angle between the propagation direction and the geomagnetic field (along which small-scale ionospheric structures tend to elongate), but otherwise ignore mean path curvature for the stochastic calculations. According to the channel probe examples given by *Nickisch* [1992] and other OTH radar validation testing we have performed [*Knepp et al.*, 2012], this approach seems adequate as long as the propagation path remains reasonably oblique (avoiding very steep refraction). However, potential effects associated with the HF sky wave reflection caustic and losses due to scattering into higher angles than the current ionosphere can refract back down are certainly being ignored in this approach.

[14] The PDM theory of *Nickisch* [1992] provides an analytical expression of the mutual coherence function for spaced frequency, position, and time in terms of sums and products over a number of phase screens defined along the propagation path. PDM also provides analytical expressions for the stochastic signal structure parameters by which the *Dana and Wittwer* [1991] General Model GPSD is parameterized. The stochastic signal structure parameters include ℓ_x and ℓ_y, the signal correlation lengths in the shortest (**x**) and longest (**y**) correlation directions orthogonal to the ray direction (these directions are defined by the ray geometry relative to the geomagnetic field and, hence, vary along the refracting HF raypath). Sometimes the designation ℓ_o is

given to ℓ_x. Two other parameters, C_{xt} and C_{yt} control the degree of spatial-temporal correlation, which in HiCIRF is determined by the direction of plasma drift relative to the raypath. The magnitudes of these parameters vary from unity for uniform plasma drift to zero for completely turbulent motion. The signal decorrelation time τ_o describes the time scale over which a signal loses coherence to the $1/e$ level. In the strong-scatter regime it is related to the signal Doppler spread by

$$\sigma_{Dop} = \frac{1}{\pi\tau_o}. \tag{1}$$

[15] The channel coherence bandwidth describes signal decorrelation in frequency (the bandwidth over which a signal can be considered to remain correlated after passage through the channel). In the work by *Dana and Wittwer* [1991] it is designated as ω_{coh}, that is, as an angular frequency. It includes both diffractive scatter of the signal by small-scale ionization structure as well as a "wander" contribution. The wander contribution alone is given by $\alpha\omega_{coh} \equiv \omega_o/\sigma_\varphi$, which defines the useful parameter α. This wander is caused by the variation of time of flight over the channel because of the variation of total electron content along the path due to the random ionization structure. The coherence bandwidth is related to the signal delay spread given by *Nickisch* [1992] by

$$\sigma_\tau = \frac{1}{\omega_{coh}}. \tag{2}$$

[16] Given the stochastic signal structure parameters, the form of the GPSD of the General Model (for a one-way path) is given by *Dana and Wittwer* [1991] as

$$GPSD(\omega_{Dop},\tau,K_x,K_y) = \frac{\pi\tau_o\ell_x\ell_y\alpha\omega_{coh}}{\sqrt{2\left(1-C_{xt}^2-C_{yt}^2\right)}}\exp\left\{-\frac{\left(\tau_o\omega_{Dop}-C_{xt}K_x\ell_x-C_{yt}K_y\ell_y\right)^2}{4\left(1-C_{xt}^2-C_{yt}^2\right)}\right\}$$
$$\times\exp\left\{-\left(\frac{K_x^2\ell_x^2+K_y^2\ell_y^2}{4}\right)-\frac{\alpha^2}{2}\left[\omega_{coh}\tau-\left(\frac{2\ell_x^4\ell_y^4}{\ell_x^4+\ell_y^4}\right)^{1/2}\left(\frac{K_x^2+K_y^2}{4}\right)\right]^2\right\} \tag{3}$$

which is a function of the Doppler frequency $f_{Dop} = \omega_{Dop}/2\pi$, delay τ, and wave numbers K_x and K_y. This form matches the PDM result of *Nickisch* [1992]. When integrated over K_x, K_y the resultant function is usually called the "scattering function,"

$$S(\omega_{Dop},\tau) = \int_{-\infty}^{\infty}\int_{-\infty}^{\infty} GPSD(\omega_{Dop},\tau,K_x,K_y)\,dK_x dK_y. \tag{4}$$

[17] The one-way GPSD is computed in HiCIRF by placing phase screens at strategic points along the numerically computed raypaths (currently, a screen is placed whenever the ray elevation angle has changed by 5°) and using the PDM formulation of *Nickisch* [1992] to calculate the stochastic signal structure parameters, where the small-scale electron density irregularity structure is defined by WBMOD. This procedure is described by *Lauer et al.* [1998, 2000], except that in HiCIRF we use a slightly different calculation for the fractional electron density variance,

$$\xi^2 = \frac{\sigma_{N_e}^2}{\langle N_e^2\rangle} = \frac{\left({}^{2\pi}/_{1000\text{meters}}\right)^{q+2}}{\int_0^{1000\,\text{km}} N_e^2\,dh}\,\frac{\Gamma(q/2-1/2)L_o^{q-1}C_{kL}}{8\pi^{3/2}\Gamma(q/2+1)}, \tag{5}$$

where q and C_{kL} are the one-dimensional spectral index and irregularity strength parameters returned by WBMOD and the irregularity outer scale size is taken to be L_o = 30 km.

[18] The channel impulse response function $h(x, y, t, \tau)$ is convolved with the transmitted signal to obtain the delayed and possibly spread signal at the receiver after propagation through the ionospheric channel,

$$E(x,y,t) = \int E_0(t-\tau)h(x,y,t,\tau)\,d\tau. \tag{6}$$

[19] Realizations of the (one-way) channel impulse response function can be generated using the technique of statistical signal generation [*Knepp and Wittwer*, 1984] using the GPSD. The procedure requires a Fourier-transformed version of the impulse response function (formally called a transfer function),

$$\tilde{h}(K_x,K_y,f_{Dop},\tau;z_R) = \iint h(x,y,t,\tau;z_R)\cdot\exp\left[i\left(K_x x+K_y y-2\pi f_{Dop}t\right)\right]dx\,dy\,dt \tag{7}$$

[20] A realization of the transfer function that is guaranteed to produce the same (ensemble averaged) GPSD is given by

$$\tilde{h}(m\Delta K_x,n\Delta K_y,j\Delta f_{Dop},k\Delta\tau) = \left[\frac{1}{\Delta K_x\Delta K_y\Delta f_{Dop}\Delta\tau}GPSD(m\Delta K_x,n\Delta K_y,j2\pi f_{Dop},k\Delta\tau)\right]^{1/2} r_{mnjk} \tag{8}$$

where the r_{mnjk} are complex Gaussian random numbers with unit variance (for convenience we have recast the GPSD in terms of frequency f_{Dop} instead of angular frequency ω_{Dop}). The K_x, K_y dimensions can be Fourier transformed to position. In HiCIRF, the user specifies the location of the

antenna phase centers through an offset array. The output of equation (8) is converted to the related quantity $h(E_i, N_i, U_i, f_{Dop}, \tau)$ for discrete f_{Dop},τ, where the E_i,N_i,U_i refer to the East-North-Up positions of the phase centers of the antenna elements given by the HiCIRF offset array. Up to details in nomenclature, this is the impulse response function of equation (6).

[21] As we mentioned, the above formulation describing what is called "micromultipath scatter" uses assumptions of strong scatter. While the strong-scatter regime is easily attained in the HF realm, it is not appropriate for most mid-latitude propagation or daylight hours in the equatorial zone. To address the weak-scatter regime in HiCIRF, we have invoked a Rician description. The idea is that for weak scatter, a substantial portion of the signal comes through with minor decorrelation. The statistical signal generation technique employed in equation (8), plus the strong-scatter theory employed in generating equation (3) (which includes a quadratic phase structure function approximation described by *Nickisch and Franke* [1996]) would mean that the signal would be overly randomized unless an appropriate coherent piece is included. This formulation separates the problem into two regimes, the scattered signal component adequately described by the strong-scatter formulation and a coherent piece. The separation between these two regimes is determined by the S_4 scintillation index, a measure of amplitude scintillation given by

$$S_4^2 = \frac{\langle I^2 \rangle - \langle I \rangle^2}{\langle I \rangle^2}, \tag{9}$$

where I is the signal intensity $I = E^*E$. *Knepp* [1982, equation (4–159)] provides a useful approximation for S_4 in terms of the phase variance σ_φ^2 σ_φ^2. (Note that we use the elongated case instead of Knepp's equation (4–158) for isotropic irregularities because elongated irregularities are more often appropriate for HF path geometries.) The approximation uses a form for S_4 valid for weak scatter,

$$S_{4,weak}^2 = 2\sigma_\varphi^2 \left[1 - \frac{1}{\left(1 + 16\xi_e^2\right)^{1/4}} \cos\left(\frac{1}{2} \tan^{-1}(4\xi_e) \right) \right] \tag{10}$$

where

$$\xi_e = \lambda P'_{ave} / \left(2\pi L_o^2\right) \tag{11}$$

and P' is the average group path distance of the phase screens from either the transmitter or the backscatter point (as appropriate). We limit the weak-scatter form of S_4 by saturating it at unity using,

$$S_4 = \tanh\left(\sqrt{S_{4,weak}^2} \right). \tag{12}$$

Then the output impulse response function is given by the sum of a coherent part v and a noncoherent part σ given by

$$v = \left(1 - S_4^2\right)^{1/4} \tag{13}$$

and

$$\sigma = \sqrt{\left(1 - \sqrt{1 - S_4^2}\right)/2}. \tag{14}$$

The output impulse response function of HiCIRF for a one-way path is then

$$h_{Dop}(E_i, N_i, U_i, f_{Dop}, \tau) = v\delta(f_{Dop})\delta(\tau) + \sigma h(E_i, N_i, U_i, f_{Dop}, \tau). \tag{15}$$

We refer to this as a Rician description in that the signal is treated as a sum of a coherent contribution and a decorrelated piece. This serves to limit the effect of the quadratic phase structure function approximation (a strong-scattering assumption) in weaker scattering environments, providing a smooth transition from the strong-scatter regime to the no-scatter regime. The intension is to capture the effect illustrated by *Nickisch and Franke* [1996, Figures 1 and 5], where the mutual coherence function (MCF) for a Gaussian phase structure function is computed with and without the quadratic phase structure function approximation, both analytically and using a finite difference time domain computation. The difference between using or not using the quadratic phase structure function approximation is the presence or absence of coherent wings at large separation values in the MCF, and this is reasonably modeled by equation (15). The Rician distribution is very similar to the Nakagami-*m* for values of the scintillation index of about 0.7 and below, so equation (15) is a good fit to both distributions currently thought to well represent ionospheric amplitude scintillation.

[22] The impulse response function for two-way paths is computed by convolution of the one-way impulse response functions for the outbound and return paths in the delay and Doppler dimensions.

[23] The Rician model used above requires further consideration in ongoing HiCIRF development. The v term at present has no phase variation caused by Total Electron Content (TEC) variations, and it is possible that a user of HiCIRF could get the wrong impression that extremely long coherent integration times could enhance the coherent term relative to the spread (σ) term. We will investigate the utility of separating the phase spectrum into small-scale-dominated and large-scale TEC effects and applying the TEC effects to vary the phase of the v term.

[24] Phase and delay for each propagation mode are calculated by ray tracing in a climatological ionosphere model. Each ray mode is then spread by the result of the stochastic calculations outlined above to incorporate disturbances from small-scale ionospheric structure. Then the phase and delay offsets are computed to account for the differences between the path lengths between different transmit and receive antenna element pairs. This procedure preserves the right phase structure from delay Doppler cell to cell, ensuring that application of signal and antenna array processing will perform correctly. The phase is further adjusted to account for ionospheric-induced Doppler shifts (by advancing the ionosphere model by 1 min and recomputing) and, in the two-way case, by ocean surface wind-generated sea Bragg backscatter spectra where appropriate (using HiCIRF's internal land-sea map). This Bragg clutter is driven by cross-calibrated multiplatform (CCMP) ocean surface wind models [*Ardizzone*, 2009] available from NASA (ftp://podaac.jpl.nasa.gov/ocean_wind/ccmp/L3.0/data/flk/).

[25] We have incorporated a computation of signal strength based on the radar equation in the two-way case and use a

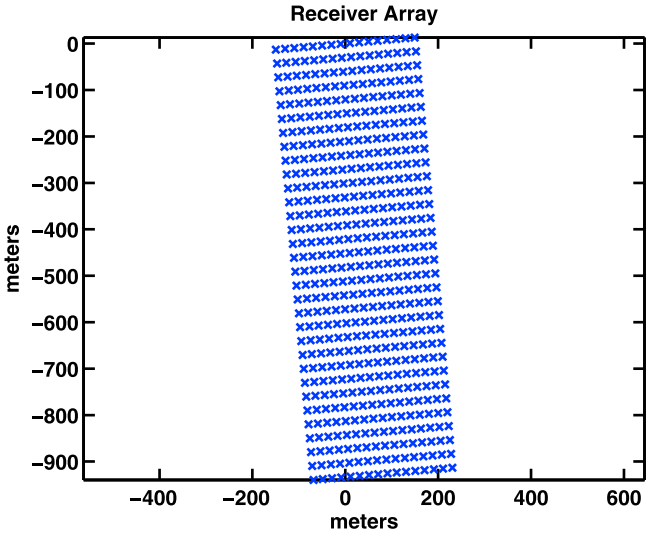

Figure 1. Sample receiver array geometry.

suitable corresponding computation for the one-way case. For the two-way case we have

$$P = \frac{P_T G_T G_R \lambda^2 \Delta A \sigma_0}{(4\pi)^3 L d_T^2 d_R^2} \tag{16}$$

where P_T is the transmitted power, G_T is the transmitter gain, G_R is the receiver gain, and λ is the transmitted wavelength. The manner in which the gain factors are applied depends on whether one is performing a multiantenna element simulation or a single element simulation representing an effective array. The backscatter coefficient σ_0 currently is a user input value for land, but for sea it is calculated using global surface wind maps. ΔA is the effective area assumed to be illuminated by a numerically traced ray and is computed using the separation of ray landing points in the simulation. The parameters d_T and d_R are effective distances along the outbound and return flux tubes [*Coleman*, 1997]. L is the path loss, which includes spreading losses (focusing and defocusing), nondeviative and deviative absorption, and ground (forward scatter) bounce losses (computed in the Coleman ray tracing code). For the one-way case, the power is computed as

$$P = \frac{P_T G_T G_R \lambda^2}{(4\pi)^2 L d_T^2}. \tag{17}$$

4. One-Way Examples

[26] The one-way version of HiCIRF simulates a sky wave communication link or HF channel probe. It can also be used for antenna array configuration design and signal processing studies. It finds propagation modes from elements at a specified transmitter location to a receiver location and generates signal realizations with micromultipath effects at specified receive array element phase centers.

[27] The "create array" tool in the HiCIRF graphical user interface can be used to lay out several types of array structures. An example of rectangular array geometry is shown in Figure 1.

[28] Our first example is a "clean" case in which no significant signal spreading is caused by the channel. The channel is from Jicamarca, Peru (the Jicamarca Radio Observatory) to Virginia. The date and time used is 15 October 2009, 0300 UT and the driving parameters are SSN = 10, Kp = 3, f = 6 MHz, CIT = 12.8 s, Bandwidth = 24 kHz. HiCIRF finds four multihop propagation modes that connect the transmitter and receiver locations, shown in Figure 2. On each of these modes, the channel scattering function is determined (the delay Doppler power spectrum of a transmitted impulse). Using *Perc* = 50% for WBMOD probability of occurrence, there is in this case no significant signal spreading and each of the four modes arrive within a single Doppler delay cell. We generated signal realizations from the HiCIRF-generated channel impulse response function and performed conventional beam forming. The result is shown in Figure 3. Note, as indicated in the caption, the beams formed at the delay of each of the incoming modes have signals arriving from the correct directions, which indicates that the simulation provides the correct signal phases at each of the receiver array element phase centers.

[29] Figure 4 displays the scattering function of the four modes when the WBMOD probability of occurrence level is set to *Perc* = 80%. In Figure 4a is the channel scattering function (corresponding to a transmitted impulse) and in Figure 4b is the amplitude-range-Doppler (ARD) plot obtained by convolving a transmitted signal with the HiCIRF Channel Impulse Response Function. ("Group Path" and "Slant Range" in Figure 4 are both synonymous with time delay times the speed of light.) With the high value of *Perc*, there is significant spread in Doppler and delay with varying degree depending on the mode. The degree to which each mode is spread depends on details of how the raypaths intersect structure in the ionosphere. In this case it is the second and fourth modes (in order of increasing delay) that happen to hit the most structured part of the ionosphere, which, though not apparent in Figure 2, occurs near 1500 km range.

[30] Next we show that antenna filtering effects [*Knepp*, 1985] are effectively produced in the one-way simulation of HiCIRF. The scattering function of Figure 4 is indicative

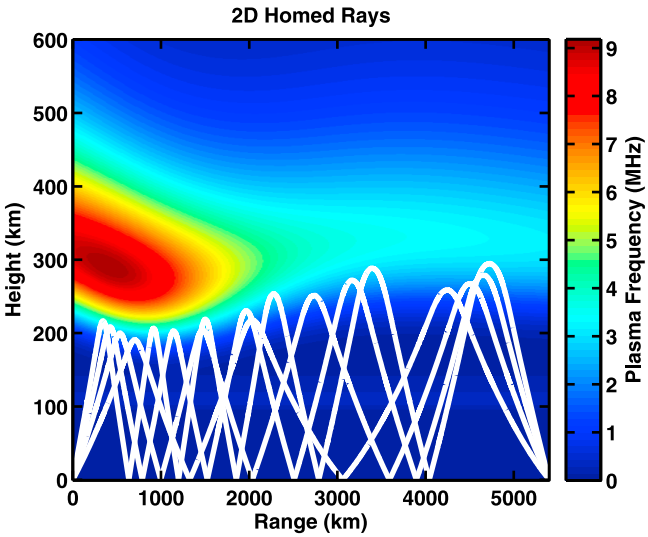

Figure 2. Four multihop modes connecting Jicamarca, Peru, and a receiver array in Virginia.

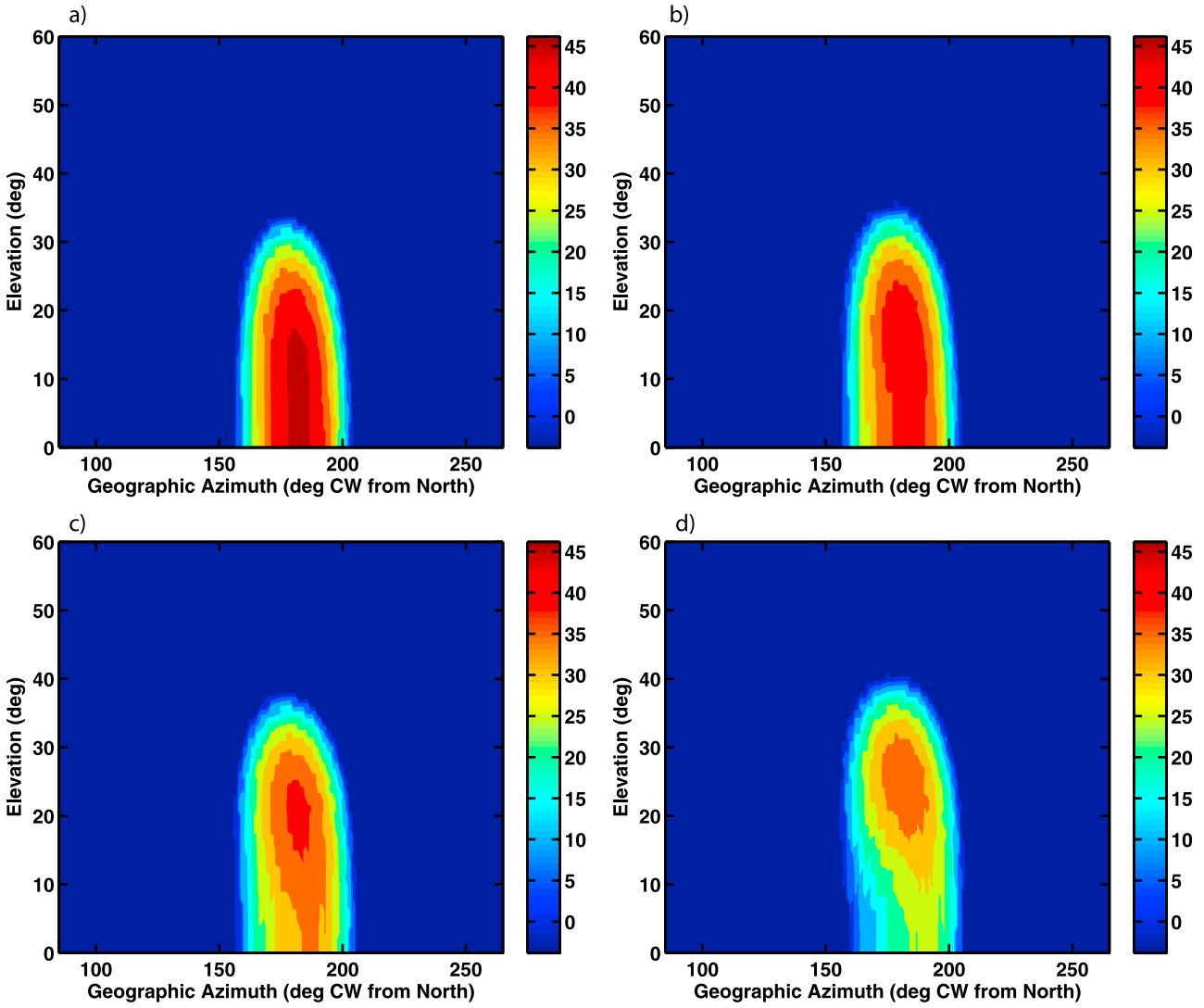

Figure 3. Conventional beam forming applied to signals generated by HiCIRF. The true azimuth of the arriving signals is 180.79°. The true elevations for the four modes are (a) 8.64°, (b) 14.43°, (c) 19.88°, and (d) 24.82°. The array of Figure 1 was used (16 × 32 elements spaced 20 × 30 m).

of fairly wide-angle scattering by small-scale ionization structure in the equatorial region. This is especially true of the fourth broadly spread mode, for which we have calculated a signal correlation distance of only 74.7 m. In fact, for the field aligned ionospheric irregularities typical of equatorial structure, the standard deviation of the angular scattering is given by

$$\sigma_\theta = \frac{\sqrt{2}}{k\ell_0} \tag{18}$$

where k is the wave number associated with the operating frequency. This implies that in our current example the fourth mode has an angular scatter standard deviation of $\sigma_\theta = 8.6°$. However, we also know that a long antenna array can form beams much narrower than this, and so we should be able to remove part of this spread by antenna filtering. Let us consider a long one-dimensional array of 300 elements separated by 7 m spacing, with boresight near the direction of the arriving signal. The azimuthal beam width for this array is approximately λ/D = 50 m/(299*7 m) * (180/π) = 1.4°. Simulating such an array and steering the beam left to right across the direct signal azimuth in steps of 16° results in the scattering functions exhibited in Figure 5. Note from Figure 5c that even when the beam is pointed directly at the source, a small amount of wing-like structure remains on the scattering function. This is due to scatter in the elevation plane that is not filtered by the narrow azimuthal beam formed by the linear array. However, the azimuthal filtering has removed much of the widely scattered signal and removes most of the power coming in at long delays (associated with the wide-angle scatter). For the beams slewed to either side, we see that the strongest incoming power tracks along the wings of Figure 4. For completeness we point out that Figure 4 corresponds to the signal received on a single element, so the results in Figure 5 benefit from the coherent

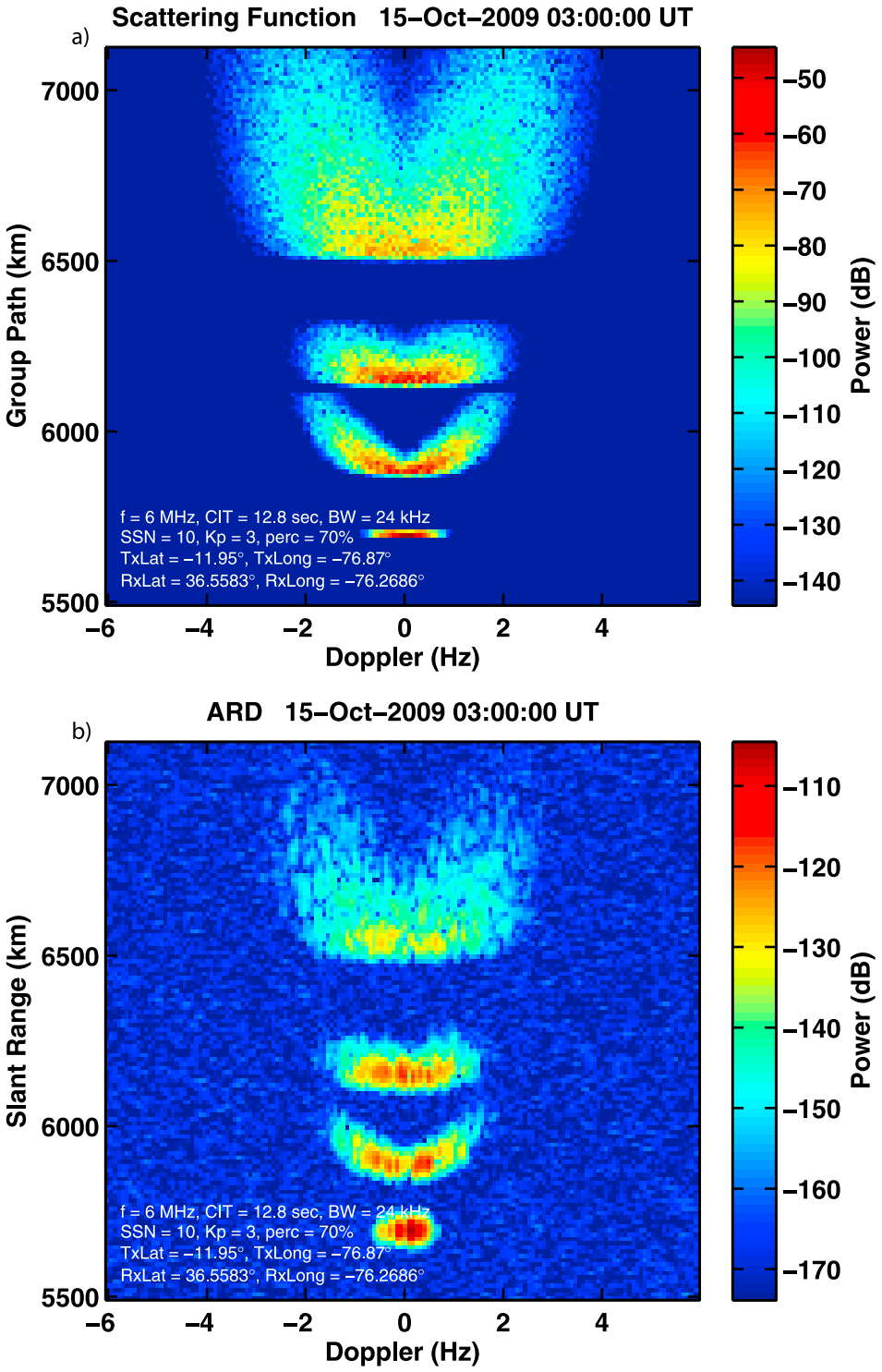

Figure 4. (a) Scattering function of the one-way channel. (b) The corresponding amplitude-range-Doppler (ARD) plot obtained by convolving with a transmitted signal and adding CCIR noise.

gain of the aperture but lose power because of the rejection of widely scattered signal components.

5. Two-Way Example

[31] The two-way radar-like geometry is significantly more difficult to implement than the one-way version reported in the previous section. To a large extent this increased difficulty is related to the necessity of accounting for propagation to all ranges and azimuths covered by the simulation and matching outbound raypaths with returning raypaths. We devised and implemented an algorithm for this matching. We then developed the capability to properly compute the two-way GPSD. Additionally, we have implemented a simplified

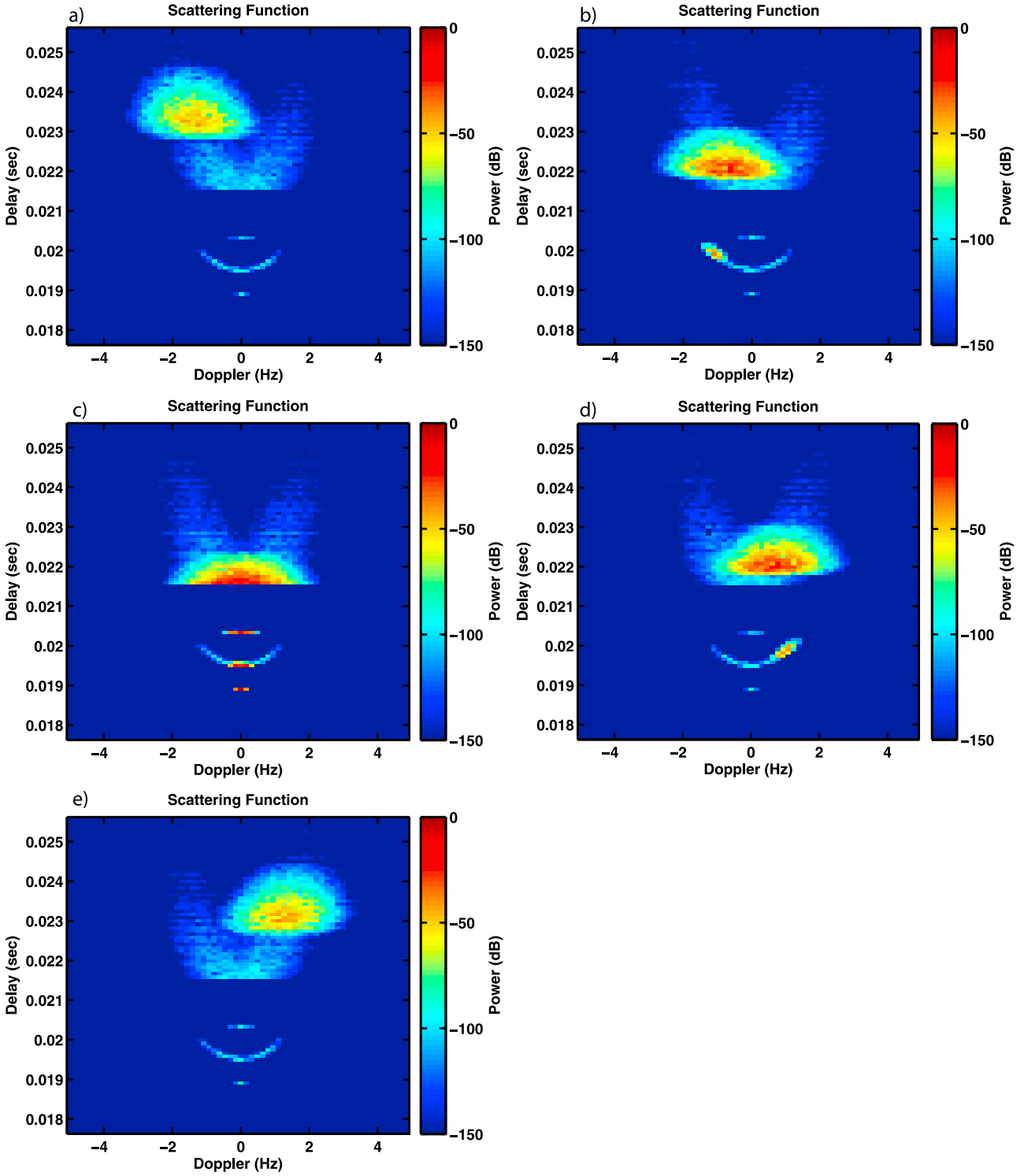

Figure 5. Antenna filtered scattering functions corresponding to a 300 element linear array with 7 m element spacing steered to (a) −32°, (b) −16°, (c) 0°, (d) 16°, and (e) 32° from the direct signal azimuth.

version of the well known CCIR noise model, we have incorporated first- and second-order Bragg scatter from the sea, and ionospheric-induced Doppler shifting is computed.

[32] Figure 6 shows a sample ARD computed using the HiCIRF two-way code for nighttime propagation exhibiting significant Spread Doppler Clutter. The azimuth of this calculation is due south from Virginia. Notice the Bragg line structure apparent in the Caribbean and the return to land clutter as the South American continent begins appearing in the returns at about 3500 km. The "fish hook" structure in the Bragg lines results from low-ray/high-ray differences in ionospheric-induced Doppler shift near the skip zone of each

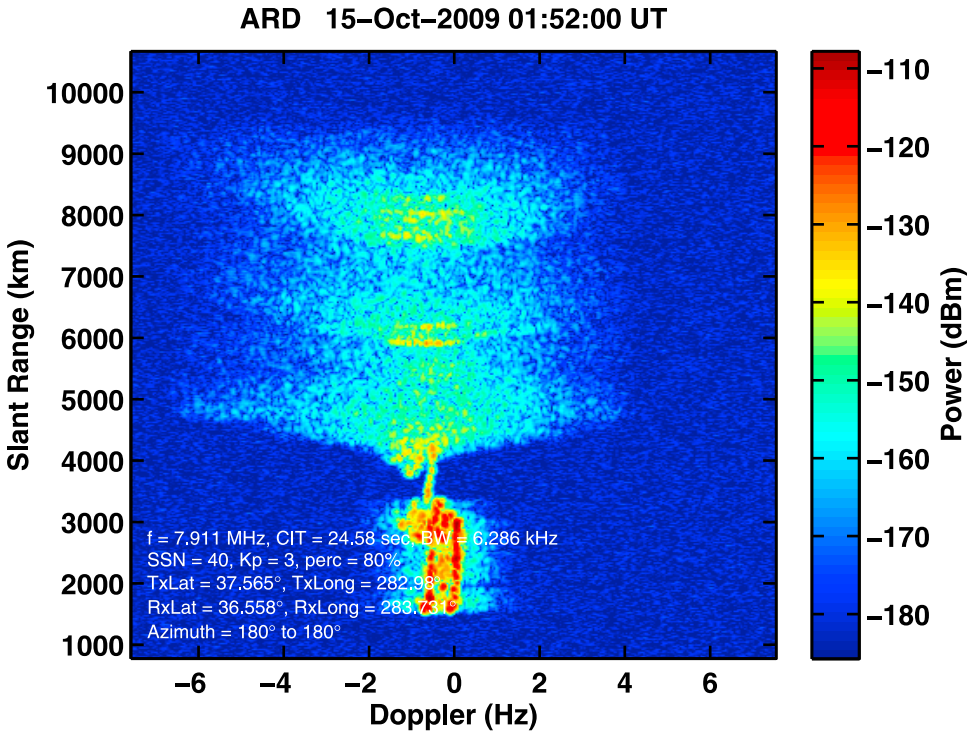

Figure 6. Sample two-way ARD for propagation due south from Virginia.

successive grouping of hops. The ground return from Cuba is evident at about 2000 km, situated between the Bragg lines. Overall, the ionospherically induced Doppler shifting is to the negative side because of the decaying nighttime ionosphere. Beyond about 4000 km slant range the ray modes become spread by equatorial small-scale ionization structure. All of these features are regularly observed in real OTH radar measurements.

6. Conclusion

[33] HiCIRF is a high-fidelity simulation of the HF sky wave propagation channel for one-way (e.g., communication or channel probe) and two-way (e.g., OTH radar) geometries that provides realistic signal generation at the antenna element level. The intention is to incorporate all relevant physics, providing a means to perform detailed system design studies like next-generation OTHR antenna array design or testing of advanced signal processing methodologies. HiCIRF synthesizes pulse-by-pulse IQ signal realizations with the appropriate phase relationships between transmit elements and receive elements, properly accounting for antenna array geometry, ionospheric refraction including multiple propagation modes, and signal scatter by small-scale ionospheric structure. Ongoing development is planned to increase HiCIRF's fidelity.

[34] A meteor clutter model for HiCIRF has recently been developed. While meteor showers such as the annual Leonid or Perseid meteor showers are well known, these are actually of less concern for OTH radar than the more-or-less constant background of "sporadic" micrometeors. We have incorporated the Meteor Input Function model (MIF) [*Fentzke et al.*, 2009]. The MIF output contains meteor realizations corresponding to the diurnal and seasonal distribution of sporadic meteors. The realizations contain meteor mass, speed, and direction as a function of geographic location and local time of day. We have developed code for generating realizations of meteor ionization trails using MIF, computing raypath intersections with individual ionization trails, and computing the OTH radar backscatter from them.

[35] In the future we will incorporate a model for direct backscatter from geomagnetic field-aligned ionization structure.

[36] The atmospheric noise model currently in HiCIRF is based on the well-known CCIR model. However, atmospheric noise at HF is quite directional in nature, and we intend to develop a directional noise model for HiCIRF. *Coleman* [2002] has pioneered the development of a directional noise model for HF. In this model, seasonal lightning strike maps serve as the directional source for atmospheric noise that is then propagated through the ionospheric waveguide to the receiver using numerical ray tracing.

[37] Another important future capability for HiCIRF will be the incorporation of a target injection utility. This will employ full three-dimensional magnetoionic ray tracing so that target signatures have the appropriate ordinary/extraordinary mode features.

[38] The Watterson Channel Model [*Watterson et al.*, 1970] has been the standard for testing HF modems for decades. How does HiCIRF compare? HiCIRF is a physics-based channel model, and is therefore capable of providing a truer representation of the ionospheric propagation channel. Instead of a user supplying mode number and delay separations, and mode spread parameters in delay and Doppler frequency, HiCIRF computes all of these from physical models. Like the Watterson Channel Model, HiCIRF can support any sampling rate; delay and Doppler frequency resolutions are controllable by the user. However, HiCIRF is

a numerically intensive application and therefore the user is advised to set the computational resolution to the minimum required to adequately sample the ionospheric effects on the signal structure and then to interpolate for higher sampling rates.

[39] **Acknowledgment.** This work was supported by AFRL under contract FA8718-09-C-0001.

References

Ardizzone, J. (2009), New multiplatform ocean wind product available, *Eos Trans. AGU*, *90*(27), 231.

Coleman, C. J. (1993), A general purpose ionospheric ray tracing procedure, *Tech. Rep., SRL0131TR*, Def. Sci. and Technol. Organ., Salisbury, South Aust., Australia.

Coleman, C. J. (1997), On the simulation of backscatter ionograms, *J. Atmos. Sol. Terr. Phys.*, *59*, 2089–2099.

Coleman, C. J. (1998), A ray tracing formulation and its application to some problems in over-the-horizon radar, *Radio Sci.*, *33*(4), 1187–1197, doi:10.1029/98RS01523.

Coleman, C. J. (2002), A direction-sensitive model of atmospheric noise and its application to the analysis of HF receiving antennas, *Radio Sci.*, *37*(3), 1031, doi:10.1029/2000RS002567.

Dana, R., and L. Wittwer (1991), A general channel model for RF propagation through structured ionization, *Radio Sci.*, *26*(4), 1059–1068, doi:10.1029/91RS00263.

Fentzke, J. T., D. Janches, and J. J. Sparks (2009), Latitudinal and seasonal variability of the micrometeor input function: A study using model predictions and observations from Arecibo and PFISR, *J. Atmos. Sol. Terr. Phys.*, *71*, 653–661, doi:10.1016/j.jastp.2008.07.015.

Gherm, V. E., N. N. Zernov, and H. J. Strangeways (2005), HF propagation in a wideband ionospheric fluctuating reflection channel: Physically based software simulator of the channel, *Radio Sci.*, *40*, RS1001, doi:10.1029/2004RS003093.

Hairston, M. R., and R. A. Heelis (1990), Model of the high-latitude convection pattern during southward IMF using DE-2 data, *J. Geophys. Res.*, *95*, 2333–2343, doi:10.1029/JA095iA03p02333.

Knepp, D. L. (1982), Propagation of wide bandwidth signals through strongly turbulent ionized media, *Tech. Rep., DNA-TR-81-78*, Def. Nucl. Agency, Washington, D. C.

Knepp, D. L. (1985), Aperture antenna effects after propagation through strongly disturbed random media, *IEEE Trans. Antennas Propag.*, *33*, 1074–1084, doi:10.1109/TAP.1985.1143491.

Knepp, D. L., and L. A. Wittwer (1984), Simulation of wide bandwidth signals that have propagated through random media, *Radio Sci.*, *19*(1), 303–318.

Knepp, D. L., L. J. Nickisch, S. V. Fridman, M. A. Hausman, and G. St. John (2010), Magnetosphere-ionosphere-thermosphere modeling—Year 1 interim report, *Interim Tech. Rep., NWRA-SEA-10-R396*, Air Force Res. Lab., Hanscom Air Force Base, Mass.

Knepp, D. L., L. J. Nickisch, S. V. Fridman, and M. A. Hausman (2011), Magnetosphere-ionosphere-thermosphere modeling—Year 2 interim report, *Interim Tech. Rep., NWRA-SEA-11–R422*, Air Force Res. Lab., Hanscom Air Force Base, Mass.

Knepp, D. L., L. J. Nickisch, S. V. Fridman, and M. A. Hausman (2012), Magnetosphere-ionosphere-thermosphere modeling—Year 3 interim report, *Interim Tech. Rep., NWRA-SEA-12-RM441*, Air Force Res. Lab., Hanscom Air Force Base, Mass.

Lauer, C., L. J. Nickisch, and W. Wortman (1998), Prediction of over-the-horizon radar clutter using the clutter effects model, *Radio Sci.*, *33*(4), 1249–1257, doi:10.1029/98RS00254.

Lauer, C., L. J. Nickisch, and W. Wortman (2000), CLEM predictions for a Puerto Rico ROTHR: Model descriptions and ionospheric structure model validation, *Tech. Rep., DSWA-TR-98-78*, Def. Threat Reduct. Agency, Fort Belvoir, Va.

Nickisch, L. J. (1992), Non-uniform motion and extended media effects on the mutual coherence function: An analytic solution for spaced frequency, position, and time, *Radio Sci.*, *27*(1), 9–22.

Nickisch, L. J., and P. M. Franke (1996), Finite difference time domain tests of random media propagation theory, *Radio Sci.*, *31*(4), 955–963.

Richmond, A. D., et al. (1980), An empirical model of quiet-day ionospheric electric fields at middle and low latitudes, *J. Geophys. Res.*, *85*, 4658–4664, doi:10.1029/JA085iA09p04658.

Rytov, S. V., Y. A. Kravtsov, and V. I. Tatarskii (1978), *Random Fields* [in Russian], *Introd. to Stat. Radiophys.*, vol. 2, Nauka, Moscow.

Secan, J. A. (2004), WBMOD ionospheric scintillation model, an abbreviated user's guide, *Rep. NWRA-CR-94 R172/Rev 7*, NorthWest Res. Assoc., Inc., Bellevue, Wash.

Watterson, C. C., J. R. Juroshek, and W. D. Bensema (1970), Experimental confirmation of an HF channel model, *IEEE Trans. Commun. Technol.*, *18*, 792–803.

C. J. Coleman, Electrical and Electronic Engineering Department, University of Adelaide, Adelaide, SA 5005, Australia.

S. V. Fridman, M. A. Hausman, L. J. Nickisch, and G. St. John, NorthWest Research Associates, 301 Webster St., Monterey, CA 93940, USA. (lj@nwra.com)